Smart Structures and Systems, *Vol. 27, No. 2 (2021) 193-207*
DOI: https://doi.org/10.12989/sss.2021.27.2.193

Non-contact monitoring of the tension in partially submerged, miter-gate diagonals

Brian A. Eick*[1], Matthew D. Smith[2a] and Billie F. Spencer[3b]

[1] *Construction Engineering Research Laboratory, U.S. Army Engineer Research and Development Center, 2902 Newmark Dr., Champaign, IL 61822, USA*
[2] *Coastal and Hydraulics Laboratory, U.S. Army Engineer Research and Development Center, 3909 Halls Ferry Rd., Vicksburg, MS 39180, USA*
[3] *Department of Civil and Environmental Engineering, University of Illinois, Urbana-Champaign, 205 N Matthews Ave, Urbana, IL 61801, USA*

(*Received March 9, 2020, Revised April 29, 2020, Accepted May 5, 2020*)

Abstract. Miter gates are water-control structures used as the damming surface on river locks and allow the water levels in the lock to raise or lower as needed. Miter gates have channel-like cross sections and are thus prone to torsional deflection due to gravity loads. To counter-act the tendency for torsional deflection and to add torsional rigidity to the gate, slender steel members termed diagonals are added across the diagonal dimension of the gate and pre-tensioned. To maintain appropriate tension in the diagonals over their lifetime, the tension in the diagonals should be monitored; however, no such monitoring is utilized. Vibration based methods to obtain an estimate of the tensile loads in the diagonal are attractive because they are simple, inexpensive, and do not require continuous monitoring. However, employing vibration-based methods to estimate the tension in the diagonals is particularly challenging because the diagonals are subjected to varying levels of submersion in water. Finding a relationship between the frequency of vibration and applied pretension that adequately addressed the effects of submersion on diagonals is difficult. This paper proposes an approach to account for the effect of submersion on the estimated tension in miter gate diagonals. Laboratory tests are conducted using scale-model diagonal specimens subjected to various levels of tension and submersion in water. The frequency of the diagonal specimens is measured and compared to an approximation using an assumed modes model. The effects of submersion on the frequency of vibration for the partially submerged diagonals are largely explained by added mass on the diagonals. Field validation is performed using a previously developed vision-based method of extracting the frequency of vibration in conjunction with the proposed method of tension estimation of an in-service miter gate diagonal that is also instrumented with load cells. Results for the proposed method show excellent agreement with load cell measurements.

Keywords: miter gates; diagonals; pre-tension; assumed modes; partial submersion; Chebyshev polynomials

1. Introduction

Miter gates are common water-control structures used as the damming surface for inland navigation lock chambers throughout the world. In the U.S., the U.S. Army Corps of Engineers (USACE) operates and maintains 237 lock chambers, of which, over 90% utilize miter gates, with two miter gate leaves necessary on each end of the lock chamber. A typical miter gate in the closed configuration is shown in Fig. 1. A miter-gate generally has a channel-like cross-section along the vertical axis where the center of gravity is offset from the shear center, as shown in Fig. 2(a). As a result, the miter-gate will tend to deflect torsionally due to its own substantial weight, as seen in Fig. 2(b). This torsional deflection can be problematic, as it will cause the gate to lean into the lock chamber and increase the likelihood that a vessel will impact and damage the gate as it enters or exits the lock chamber. Moreover, the miter gate structure (without diagonals) is generally considered to have negligible torsional stiffness. Without the tensioned diagonals, the components of the miter gate will be subjected to excessive torsional stresses due to hydrodynamic forces when the gate swings open and closed through water. To counteract the tendency of the gate to twist under its own weight and to add some torsional stiffness, pre-tensioned diagonals are added to the gate, as shown in Fig. 2(c). Formulas to determine the appropriate pretension for the diagonals were developed by Hoffman (1944) and Shermer (1957), and are summarized in the engineer design manual utilized by the USACE for miter gate design, EM 1110-2-2703 (U.S. Army Corps of Engineers 1994). Utilizing Hoffman (1944) and Shermer (1957), pretension in the diagonals is selected so that the gate will hang plumb, and the diagonals will never decompress when the gate is subjected to any torsional load.

*Corresponding author, Ph.D.,
E-mail: brian.a.eick@erdc.dren.mil
[a] Ph.D., E-mail: matthew.d.smith@erdc.dren.mil
[b] Professor, E-mail: bfs@illinois.edu

ISSN: 1738-1584 (Print), 1738-1991 (Online)

Fig. 1 Miter gate at Lock 27 on the Mississippi River with partially submerged diagonals shown

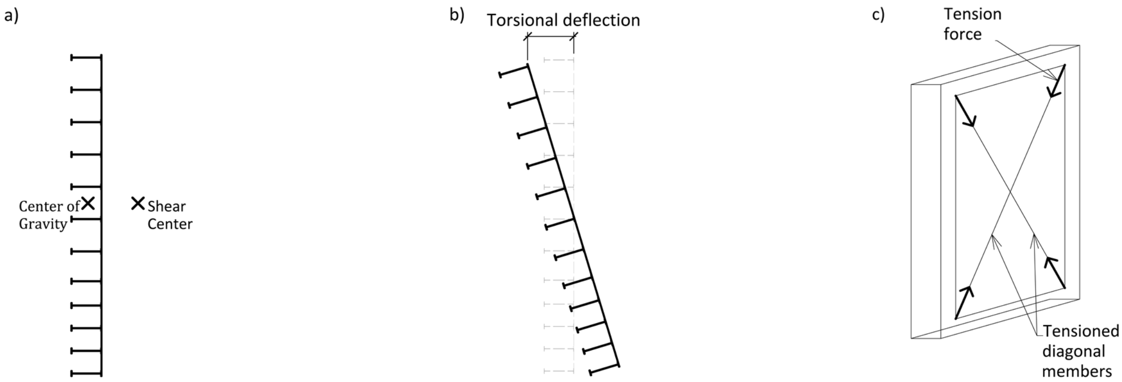

(a) Eccentricity between center of gravity and shear center

(b) Torsional deflection due to self-weight of gate

(c) Tensioned diagonals added to counter-act torsional deflection

Fig. 2 Function of miter gate diagonals

Maintaining appropriate tension in the diagonals is of critical importance to maintaining the operability and extending the usable life of the miter gate. Inappropriate tension in the diagonals may cause the gate to lean into the chamber, increasing the likelihood of impact from passing vessels. This type of inappropriate tension may manifest itself as an obvious lean of the gate, signifying an issue in diagonal tension. However, it is possible that the miter gate diagonals will have an appropriate combination such that the gate will hang plumb, but have either insufficient tension to resist the torsional loads caused by gate swings, or excessive tension causing yielding in the diagonals when resisting torsional loads. This type of inappropriate diagonal tension of may lead to accelerated fatigue damage due to stresses beyond the design limits (Riveros *et al*. 2017), and would not manifest itself readily with obvious changes in the gate. Monitoring the tension in the diagonals using direct measurements such as strain gages or load pins would be straightforward; however, the majority of diagonals are already in service without instrumentation installed. Placing, for example, strain gages on the in-service diagonals will only allow monitoring of future changes in strain, rather than providing an indication of the magnitude of tensile stress in the component. Moreover, the infrastructure necessary to utilize strain gages or load pins, such as cabling and data acquisition hardware, does not exist on most miter gates and would be prohibitively expensive to install. Accordingly, there is growing interest in using vibration-based monitoring to infer the tension in the diagonals from a measured frequency of vibration. Many researchers have used vibration-based techniques to monitor the tension in structural components (Rytter 1993), with a particular focus on cables of cable-stayed bridges (Jang *et al*. 2010, Feng *et al*. 2017, Kim and Kim 2013). Work has also been done on inferring damage in cables that may be manifested in modal properties due to changes in stiffness or tension (Lepidi *et al*. 2007, 2009). Eick *et al*. (2020), investigated the feasibility of non-contact, vision-based monitoring of the tension in miter gate diagonals by using video of a vibrating diagonal. The vision-based method proposed by Eick *et al*. (2020), utilizes a technique known as Lukas-Kanade optical flow to track the displacement of the vibration of a manually selected location on the miter gate diagonal. Once the displacement

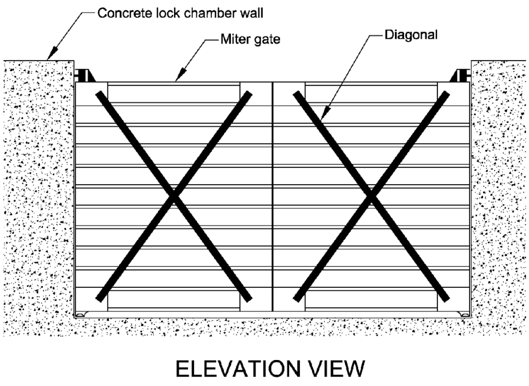

(a) Elevation view showing diagonals

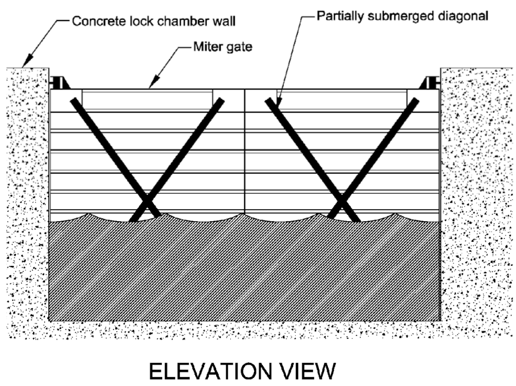

(b) Elevation view showing typical, partially-submerged condition of diagonals

Fig. 3 Elevation views of miter gates

record is obtained, a fast Fourier-transform (FFT) is performed on the record to obtain the frequencies of vibration. In laboratory tests, Eick *et al*. (2020), found excellent agreement between the frequencies of vibration of scale-model diagonal specimens measured using accelerometers and those measured using the vision-based method.

A particular challenge to vibration-based monitoring of miter-gate diagonals is that they are subjected to varying amounts of submersion in water. Fig. 3(a) shows an elevation view of a typical miter gate, while Fig. 3(b) shows the typical in-situ partially submerged condition of a miter gate. Draining, or “dewatering” a lock chamber requires specialized infrastructure to be put in place and is thus very expensive; dewaterings are only performed infrequently for routine maintenance once every five to ten year, or for emergency repairs to prevent catastrophic failure of the gate. Generally speaking, the diagonals on a miter gate will be partially submerged for the vast majority of their life.

Little literature is available on monitoring the tension in fluid-structure interaction systems akin to miter gate diagonals, particularly for partially submerged structures. The aforementioned study by Eick *et al*. (2020), utilized flowing water to excite scale model diagonals to obtain frequencies of vibration under conditions that might be expected in the field. The flowing water was induced by filling a submersion chamber with water. Eick *et al*. (2020) found that as the submersion chamber of the scale model diagonal specimens filled with water, and the specimens became more submerged, the frequency of the diagonal tends to decrease. Indeed, by not accounting for the effects of submersion on the diagonal, tension calculations based on the frequency of vibration of a miter gate diagonal will be underestimated. A great deal of literature is available on fluid-structure interaction systems and the effects on vibration frequency, such as Chen (1985). Generally, the discussions in the literature are for fully submerged structures. Miter gate diagonals are typically partially submerged, and the amount of submersion can vary significantly due to seasonal variations in the river levels. Chen (1985) suggests that, for a beam in an ideal fluid, the primary effect of submersion on a vibrating beam is a reduction in frequency that can be modeled as added mass to the system; in general, submersion can also cause increased damping and changes in stiffness of the fluid-structure system. It is unclear if a miter gate diagonal can be appropriately modeled as vibrating in an ideal fluid. Moreover, much of the literature provides results for prismatic beams, which miter gate diagonals are not.

This paper proposes an approach to account for the effect of submersion on the estimated tension in miter gate diagonals. A laboratory experiment utilizing scale-model diagonal specimens is utilized to obtain the vibrating frequencies of the diagonals subjected to various tensions and levels of submersion. The results of Chen (1985), regarding the modeling of the effects of submersion on the frequency of vibration of a beam as added mass are investigated. Using the approximate assumed modes method, frequencies of vibration for the tensioned beam are generated considering the added mass due to submersion. An experimental procedure is then devised to measure the frequency of vibration of partially submerged beams with accelerometers using a hammer impact test. The frequencies generated using the proposed approximate approach are compared to the experimental data, and the effects of partial submersion are shown to be adequately explained by considering added mass due to the volume of water displaced as the diagonals vibrate. Finally, the proposed method is validated in the field on the vibrating diagonals on the miter gate at the Greenup Lock and Dam. Due to difficultly in physically accessing the diagonals in the field, the video-based approach described by Eick *et al*. (2020) is utilized. Using a video of the vibrating diagonals on the miter gate at the Greenup Lock and Dam, the displacement record of the vibrating diagonals is found via Lukas-Kanade optical flow by manually selecting a pixel in the first frame of a video to track. Optical flow then iterates through the frames of the video to track the apparent displacement of the track pixel. The tracked displacement is stored, and a fast Fourier transform is used to obtain the frequencies of vibration. The calculated tension using the proposed method with the measured frequency is compared with readings from an installed load-cell on the diagonal, showing excellent agreement. The specifics of the vision-based monitoring approach to diagonal tension monitoring can be found in Eick *et al*. (2020).

2. Vibrating beam dynamics

Miter gate diagonals are long and very slender beams. Relationships can easily be found to relate the geometry of the beam to the frequencies of vibration. These relationships become more complicated when the beam is tensioned; nevertheless, the relationship between beam geometry, tension, and frequencies of vibration are readily available in the literature, such as the compilation by Shaker (1975). The general solution to the equation of motion of a tensioned, prismatic, Euler-Bernoulli beam is given in generalized non-dimensional form as follows

$$v(\bar{x}) = C_1 \cosh(\alpha_1 \bar{x}) + C_2 \sinh(\alpha_1 \bar{x}) + C_3 \cos(\alpha_2 \bar{x}) + C_4 \sin(\alpha_2 \bar{x}) \quad (1)$$

where

$$\alpha_1 = \left(\frac{k^2}{2} + \sqrt{\frac{k^4}{4} + \beta^4} \right)^{\frac{1}{2}} \quad (2)$$

$$\alpha_2 = \left(-\frac{k^2}{2} + \sqrt{\frac{k^4}{4} + \beta^4} \right)^{\frac{1}{2}} \quad (3)$$

$$k = \sqrt{\frac{PL^2}{EI}} \quad (4)$$

$$\beta = L \left(\frac{\mu \omega^2}{EI} \right)^{\frac{1}{4}} \quad (5)$$

$$\bar{x} = \frac{x}{L} \quad (6)$$

where E is the beam's modulus of elasticity, L is the length of the beam, I in the moment of inertia of the beam in the direction of vibration, x is the location on the beam from the datum, and μ is the mass per unit length of the beam. P is the axial tensile load in force units while ω is the frequency of vibration. C_n are constants of integration that are determined using the boundary conditions of the problem. The characteristic equation of the beam is found by solving for the constants of integration, which is done by taking the determinate of the matrix that consists of the coefficients for the unknowns based on the boundary conditions. Eq. (1) assumes small amplitude vibrations, which is reasonable for a miter gate diagonal. For this study, it is further assumed that thermal loadings due to changes in temperature are negligible. This simplification is reasonable as the measurements used to calculate tension are taken over a period of one minute, where changes in temperature will be insignificant. Eick *et al*. (2020) found that miter gate diagonals that utilize super-nut style connectors are most appropriately modeled as fixed-pinned, in which case, the characteristic equation of the beam is as given by

$$\alpha_1 \cosh \alpha_1 \sin \alpha_2 - \alpha_2 \sinh \alpha_1 \cos \alpha_2 = 0 \quad (7)$$

For a pinned-pinned beam, the characteristic equation is given by

$$\sin \alpha_2 = 0 \quad (8)$$

With the characteristic equation in hand, the tension in the beam can be determined if the geometry, material properties, and frequency of vibration are known.

2.1 Effects of submersion on the vibrating frequency of a beam

Fluid-structure interaction systems consist of a structure moving through a fluid, a volume of which must be displaced to allow the structure to move. For simplicity, consider an illustrative example of a single-degree-of-freedom (SDOF) structure. In the fluid-structure interaction system, the structure itself has some stiffness (k_s), mass (m_s), and damping (c_s). The fluid also has some stiffness (k_a), mass (m_a), and damping (c_a). The subscript a is used here for "added", in that the values from the fluid are thought of as added to the structure. The formulation of the equation of motion for an SDOF fluid-structure interaction system then takes the form outlined in Kaneko *et al*. (2014) as

$$(m_s + m_a)\ddot{x} + (c_s + c_a)\dot{x} + (k_s + k_a)x = f \quad (9)$$

Chen (1985) notes that, for a structure moving through an at-rest, ideal fluid (i.e., incompressible and inviscid), the primary effect of the submersion is to add mass, and so Eq. (9) can be simplified to

$$(m_s + m_a)\ddot{x} + c_s\dot{x} + k_s x = f \quad (10)$$

The experimental analysis performed herein shows that, for determining the effects of submersion on the fundamental frequency of vibration of a beam, the simplification provided in Eq. (10) produces excellent results. Care should be taken in the field to ensure the water surrounding a miter gate diagonal is, indeed, at rest, Testing should not be performed when a vessel is passing the gate, or if both lock gates are open allowing flow through the lock chamber. The value of added mass can be determined analytically and is related to the geometry of the structure, which dictates the volume of water displaced when the structure moves through the fluid, and the properties of the fluid. Tabulated values of added mass for common geometries are available in the literature, such as in Kaneko *et al*. (2014). For this study, the geometry of the diagonals closely resembles a thin plate in two cases studied and a rectangular prism in one case. The value of added mass per unit length of a thin plate of width $2a$ is given by

$$\mu_{a\_plate} = \rho_{water} \pi a^2 \quad (11)$$

The value of added mass for a rectangular prism of width $2a$ and depth $2b$ is dependent on the aspect ratio of the cross section, b/a. As will be seen the rectangular geometry used in this study has an aspect ratio of 0.57. Using the table available in Kaneko *et al*. (2014) and linearly interpolating, the value of added mass per unit length for the rectangular prism used in this study is given by

$$\mu_{a\_rectangle} = 1.38\rho_{water}\pi a^2 \tag{12}$$

If the beam is fully submerged in water, then the same approach as above can be used to find the relationship between the frequency of vibration and tension, with the note that Eq. (5) becomes

$$\beta = L\left(\frac{(\mu+\mu_a)\omega^2}{EI}\right)^{\frac{1}{4}} \tag{13}$$

2.2 Modeling a partially submerged miter gate diagonal

A challenge in this study is the fact that the diagonals will generally only be partially submerged, and so, the added mass due to water will only act on the submerged portion of the diagonal. The diagonals on a miter gate can thus be modeled as piecewise beams with two distinct sections. The first section has a length, L_w, corresponding to the submerged part of the beam and has a mass per unit length of the steel plus the added mass per unit length due to water. The other section has length corresponding to the unsubmerged length of the beam and mass per unit length of steel only. On both sections of the beam, all other geometric and material properties are the same. The beam model for a partially submerged diagonal for the pinned-pinned case is shown in Fig. 4.

The relatively simple adjustment to the continuous beam model of adding mass to a portion of the beam leads to a complicated closed-form relationship between the tension in the beam and the frequency of vibration. For the beam shown in Fig. 4, the characteristic equation of the beam is given by the determinant of the matrix below

$$\begin{bmatrix} \sinh\left(\alpha_{1a}\frac{L_w}{L}\right) & \sin\left(\alpha_{2a}\frac{L_w}{L}\right) & -\cos\text{h}\left(\alpha_{1b}\frac{L_w}{L}\right) & -\sinh\left(\alpha_{1b}\frac{L_w}{L}\right) & -\cos\left(\alpha_{2b}\frac{L_w}{L}\right) & -\sin\left(\alpha_{2b}\frac{L_w}{L}\right) \\ \alpha_{1a}\cosh\left(\alpha_{1a}\frac{L_w}{L}\right) & \alpha_{2a}\cos\left(\alpha_{2a}\frac{L_w}{L}\right) & -\alpha_{1b}\sinh\left(\alpha_{1b}\frac{L_w}{L}\right) & -\alpha_{1b}\cosh\alpha_{1b}\frac{L_w}{L} & \alpha_{2b}\sin\left(\alpha_{2b}\frac{L_w}{L}\right) & -\alpha_{2b}\cos\left(\alpha_{2b}\frac{L_w}{L}\right) \\ \alpha_{1a}^2\sinh\left(\alpha_{1a}\frac{L_w}{L}\right) & -\alpha_{2a}^2\sin\alpha_{2a}\frac{L_w}{L} & -\alpha_{1b}^2\cosh\alpha_{1b}\frac{L_w}{L} & -\alpha_{1b}^2\sinh\alpha_{1b}\frac{L_w}{L} & \alpha_{2b}^2\cos\alpha_{2b}\frac{L_w}{L} & \alpha_{2b}^2\sin\alpha_{2b}\frac{L_w}{L} \\ \alpha_{1a}^3\cosh\alpha_{1a}\frac{L_w}{L} & -\alpha_{2a}^3\cos\alpha_{2a}\frac{L_w}{L} & -\alpha_{1b}^3\sinh\alpha_{1b}\frac{L_w}{L} & -\alpha_{1b}^3\sinh\alpha_{1b}\frac{L_w}{L} & -\alpha_{2b}^3\sin\alpha_{2b}\frac{L_w}{L} & \alpha_{2b}^3\cos\alpha_{2b}\frac{L_w}{L} \\ 0 & 0 & \cosh(\alpha_{1b}) & \sinh(\alpha_{1b}) & \cos(\alpha_{2b}) & \sin(\alpha_{2b}) \\ 0 & 0 & \alpha_{1b}^2\cosh\alpha_{1b} & \alpha_{1b}^2\sinh\alpha_{1b} & \alpha_{2b}^2\cos\alpha_{2b} & \alpha_{2b}^2\sin\alpha_{2b} \end{bmatrix}$$

where α_1 and α_2 are as described in Eqs. (2) and (3), but the subscripts *a* and *b* refer to using the appropriate material and geometric properties of the bottom and top sections of the beam, respectively, as shown in Fig. 4. The determinant can be explicitly found using appropriate symbolic math software; however, determining the tension given a specified measured frequency of the beam is not possible in closed form and must be done numerically.

Because of the ease of implementation and computational efficiency, the assumed modes method (Craig and Kurdila 2006) is employed to model the submerged beam. For the assumed modes method, admissible shape functions must be selected for the *n* modes to be estimated. Here, we refer to the *i*th shape function as ψ_i. An admissible shape function is one that satisfies the geometric boundary conditions of the beam and is twice differentiable. Moreover, each of the n assumed mode shape functions must be linearly independent of all other assumed mode shape functions. To determine the frequencies of vibration using the assumed modes method, the eigenvalue problem is solved such that

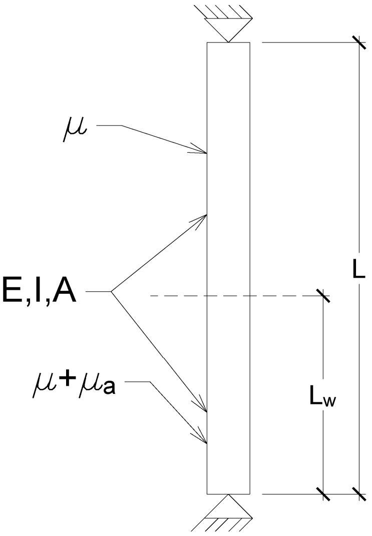

Fig. 4 Piecewise beam model for partially submerged miter gate diagonal

$$det\Big(\big([K_{stiff}]+[K_{geom}]\big) - \omega^2\big([M_{beam}]+[M_{added}]\big)\Big) = 0 \tag{14}$$

where $[K_{stiff}]$ is the bending stiffness matrix of the beam, $[K_{geom}]$ is the geometric stiffness matrix of the beam, $[M_{beam}]$ is the mass matrix of the beam, and $[M_{added}]$ is the added mass matrix of the beam. Note, the damping of the beam itself is assumed negligible and as stated previously, the results from Chen (1985) are first explored by only considering the added mass of the water. The *i*, *j* component of each of these matrices is found as in Eq. (15) through Eq. (18)

$$K_{stiff_{i,j}} = \int_0^L EI(x)\psi_i''(x)\psi_j''(x)dx \tag{15}$$

$$K_{geom_{i,j}} = \int_0^L P\psi_i'(x)\psi_j'(x)dx \tag{16}$$

$$M_{beam_{i,j}} = \int_0^L \mu\psi_i(x)\psi_j(x)dx \tag{17}$$

$$M_{added_{i,j}} = \int_0^{L_w} \mu_a\psi_i(x)\psi_j(x)dx \tag{18}$$

Where the "prime" superscript denotes the derivative of the shape function with respect to the dimension along the length, *x*. The frequencies calculated using Eq. (14) will be higher than the true frequency of the beam being modeled; however, the estimate will converge from above toward the true value as the number of assumed modes increases (Rao 2007).

To satisfy the requirement for linear independence while providing a reasonable estimate of the mode shapes of a beam, trigonometric functions are frequently employed. However, to get sufficiently converged results, many such mode shapes may need to be considered in the formulation, leading to a computationally demanding problem. To increase computational efficiency, the authors herein consider the use of so-called Chebyshev polynomials of the first kind (for brevity, herein simply referred to as Chebyshev polynomials). Chebyshev polynomials, denoted $T_n(x)$, are closely related to the cosine function (Mason and Handscomb 2003), in that

$$T_n(x) = \cos\big(n \arccos{(x)}\big), x \in [-1,1] \tag{19}$$

As seen, Chebyshev polynomials take the form $\cos n\theta$, and so each *n*th Chebyshev polynomial is linearly independent. Using Rodrigues' formula, the *n*th Chebyshev polynomial can be found as

$$T_n(x) = \frac{(-2)^n n!}{(2n)!}\sqrt{1-x^2}\frac{d^n}{dx^n}(1-x^2)^{n-\frac{1}{2}} \tag{20}$$

For example, when $n = 5$

$$T_5(x) = 16x^5 - 20x^3 + 5x \tag{21}$$

The Chebyshev polynomials are closely related to the cosine function on the interval [-1,1], and so, for this study this relationship is shifted to lie in the desired interval [0,L] by using the argument $\left(\frac{2x}{L}-1\right)$. The Chebyshev polynomials themselves do not satisfy the requirements for an admissible shape function. For this study, as per Eick *et al*. (2020), the beam is best modeled as fixed-pinned, and so the shape functions must satisfy $\psi_i(0) = 0$, $\psi_i(L) = 0$, $\psi_i'(0) = 0$, and $\psi_i'(L) \neq 0$. To satisfy the boundary conditions, two terms are added to each nth Chebyshev polynomial such that ith shape function is defined as in Eq. (22), which for every i^{th} mode of vibration of can be shown to be an admissible shape function.

$$\psi_i(x) = \left(\frac{x}{L}\right)^2\left(1-\frac{x}{L}\right)T_i\left(\frac{2x}{L}-1\right) \tag{22}$$

The benefit of using the Chebyshev polynomial, as opposed to trigonometric functions, is in significantly increased computational efficiency of integrating simple polynomials in Eqs. (15) through (18). For this study, it was found that using 20 mode shapes in the formulation provides sufficiently converged results.

The assumed modes formulation allows the estimation of the frequency of vibration of a beam given all the relevant parameters. For this study, it is of interest to estimate the tension in beam, given a measured frequency and all other necessary parameters for the problem. For a miter gate diagonal, geometric and material properties are obtained from structural design drawings. Then, measurements must be taken to obtain the frequencies of vibration and the length over which the diagonal is submerged. The assumed modes formulation is setup then with the only unknown being P in Eq. (16). P can reasonably be assumed constant throughout the beam, and so it is taken out of the integral and geometric stiffness matrix is kept in terms of P. Eq. (14) is calculated by iterating through P until a frequency value is obtained within a small percentage of error of the frequency measured in the field (say 1%). For this initial study, only the fundamental frequency is considered, with results being shown to be sufficiently accurate. Future work will investigate the potential for increased accuracy by including results from multiple modes of vibration.

3. Experimental setup

An experimental setup was devised to demonstrate the performance of the proposed method. Scale model diagonal specimens subjected to various levels of submersion and tension were tested. The experiment was comprised of three scale-model diagonal specimens with dimensions as shown in Fig. 5. The cross sectional dimension *a* and *b* seen in Fig. 5 are listed in Table 1. The cross-section of each specimen was chosen such that each specimen has identical cross-sectional area of 11.3 cm^2 (1.75 in^2) while allowing for varying profile widths moving in the water. The geometry of the scale model specimens, with an end section tapering from a rectangular cross section to a round threaded rod, is typical of many miter gate diagonals. The threaded end sections are provided to allow for connectivity in the form of a heavy hex nut on one end and a super-nut-style multi-jack-bolt tensioning nut on the other end, which is used to provide the pre-stress.

The specimens were erected vertically and attached to the structural reaction wall and load floor in the laboratory. A submersion tank was constructed out of four welded 208-liter (55 gallon) drums stacked on top of each other and erected around each specimen. The submersion tank allowed for the partial submersion of the specimens. Each specimen had three strain gages attached to obtain a reference value of tension, and two accelerometers were placed just above the submersion chambers, which is offset from the mid-span by about 20 cm. The location of accelerometers was selected to facilitate the maximum number of measured modes by avoiding modal zeros (locations where displacements are expected to be zero for the first few modes). Note, for the laboratory experiments, accelerometers (as opposed to the vision-based method) are

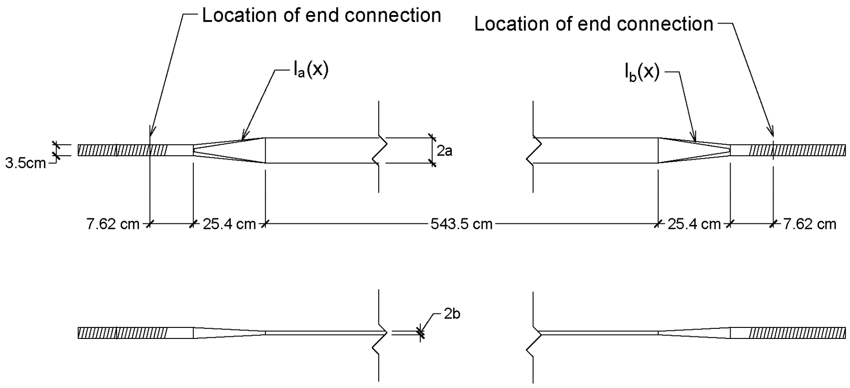

Fig. 5 Scale model diagonal specimens used in this test

Table 1 Scale model diagonal specimens

Name	Cross sectional dimensions
Specimen 1	a = 8.89 cm (3.50 in), b = 0.32 cm (0.13 in)
Specimen 2	a = 4.45 cm (1,75 in), b = 0.64 cm (0.25 in)
Specimen 3	a = 2.22 cm (0.88 in), b = 1.27 cm (0.5 in)

exclusively used for dynamic measurements. This is because of the ability to capture higher modes with the accelerometers. As outlined by Eick *et al*. (2020) a typical camera with a frame rate of 60 frames per second (fps) will have Nyquist frequency of 30 Hz. For the specimens used in this study, 30 Hz is only sufficient to capture two or three

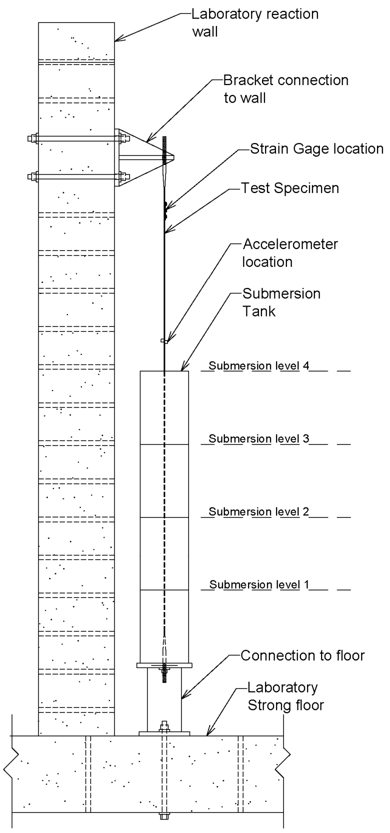

Fig. 6 Experimental setup

Fig. 7 Erected test specimen with submersion chamber

modes for each beam. Nevertheless, the study performed by Eick *et al*. (2020) readily shows that the vision-based method can match accelerometers nearly exactly over the range of measurement. A schematic of the experimental setup in the lab is shown in Fig. 6. Fig. 7 shows the erected test specimen in the lab.

To determine its fundamental frequency, the specimen was excited and the response was recorded using both video and accelerometers. In the course of testing at certain levels of submersion, exciting the lower modes with a hammer impact proved difficult; using a small rope tied near the center of the specimen plucking the specimen provided best results. Each specimen was tested at five different tension levels as listed in Table 2. For each level of stress, the beam was submerged to five different levels as listed in Table 2. Thus, a total of 25 tests were performed for each of the three specimens. For simplicity, the height of the individual 208 liter (55 gallon) drums were used as a marker for each level of submersion, with each drum being approximately 83.8 cm (33 in.) tall. When testing, the expected fundamental frequency of vibration for all tests is not expected to exceed 14 Hz, and so a sampling frequency of 256 Hz was selected

Table 2 Tensile stresses and water heights utilized in testing

Tensile stress levels	38.92, 77.84 116.77 155.69 194.6 kN (8.75, 17.5, 26.25, 35.0, 43.75 kips)
Height of water	0, 83.8, 167.6, 251.5, 335.3 cm (0, 33, 66, 99, 132 in.)

for the accelerometers, which will allow for the measurement of several harmonics for each test. To obtain the frequencies of vibration, a fast Fourier-transform (FFT) is performed on the recorded acceleration record, and peaks in the record are manually selected.

4. Model validation

For each test, up to the first five frequencies of vibration are extracted from the FFT of the acceleration record. Note that in several instances, the frequencies of a particular harmonic of the beam's vibration are difficult to determine from the FFT, possibly due to the frequency of that harmonic nearly resonating with the frequency of vibration of the global test setup. In other instances, the amplitude of a particular harmonic is quite small, likely due to the placement of the accelerometer near the node for that mode of vibration. An example of an FFT displaying both of these characteristics (closely spaced peaks, and very low amplitude peak), is shown in Fig. 8, which is the amplitude spectrum for specimen 1 at 155.69 kN (35 kips) stress and with 335 cm (132 in) of water. The numbers in the plot correspond to the frequency of the n^{th} mode of vibration, as determined by a peak-picking algorithm. In this case, several closely spaced peaks are seen near where the second mode is expected. Similarly, the amplitude for the peak near where the fifth mode is very small. Accordingly, for this test, the second and fifth modes cannot be determined and are marked as N/A.

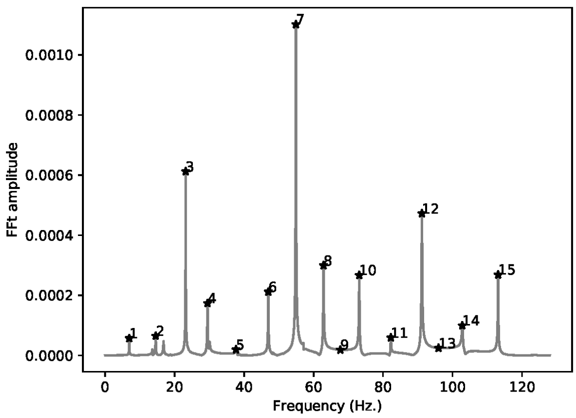

Fig. 8 Amplitude spectrum for test specimen 1 at 137.9 MPa (20 ksi) and 335.3 cm (132 in) of water

To validate the notion that added mass is the primary driver for a change in the frequency of vibration, the extracted frequencies from the experimental data are compared to the frequencies calculated using the proposed approach. Note, for specimens 1 and 2, the added mass to use in Eq. (18) is the value for a thin plate (Eq. (11)). For specimen 3, the aspect ratio of the cross-section is a rectangular prism, and so the added mass from Eq. (12) is used. For all specimens, the bending stiffness varies across the length of the bar due to the changing cross section, as seen in Fig. 5. Taking the left end connection shown in Fig. 5 as the datum, each specimen is comprised of the following: a circular cross-section from 0 cm to 7.62 cm; a tapered region with varying cross section from 7.62 cm to 33.0 cm; a constant rectangular cross section from 33.0 cm to 576.5 cm; a tapered region with varying cross-section from 576.5 to 601.9 cm; a constant circular cross section from 601.9 cm to 609.5 cm. The moments of inertia from the regions with constant cross section are readily obtained from the dimensions in Table 1. The moments of inertia for the tapered sections, labeled $I_a(x)$ and $I_b(x)$ in Fig. 5, are functions of the position on the beam, x, and thus need to be incorporated into the integral in Eq. (15). Approximate functions describing $I_a(x)$ and $I_b(x)$ with respect to the datum previously described are listed in Table 3.

Figs. 9 through 11 show a comparison between the calculated frequencies from the proposed method and the experimentally measured frequencies. In the plots, the x-axis represents the calculated frequencies using the method of assumed modes, while the y-axis represents the experimentally measured frequencies. A line is also

Table 3 Functions describing the varying moment of inertia of the tapered section for the test specimens

Specimen	Functions of $I_a(x)$ and $I_b(x)$ (x in cm)
1	$I_a(x) = \frac{1}{12}(0.567x - 0.966\ cm)(-0.107x + 4.178cm)^3$ $I_b(x) = \frac{1}{12}(-0.567x + 345.112\ cm)(0.107x - 61.225cm)^3$
2	$I_a(x) = \frac{1}{12}(0.217x + 1.701\ cm)(-0.082\ x + 3.987\ cm)^3$ $I_b(x) = \frac{1}{12}(-0.217x + 134.419\ cm)(0.082x - 46.175\ cm)^3$
3	$I_a(x) = \frac{1}{12}(0.043x + 3.035\ cm)(-0.032x + 3.606\ cm)^3$ $I_b(x) = \frac{1}{12}(-0.043x + 29.072\ cm)(0.032x - 16.076\ cm)^3$

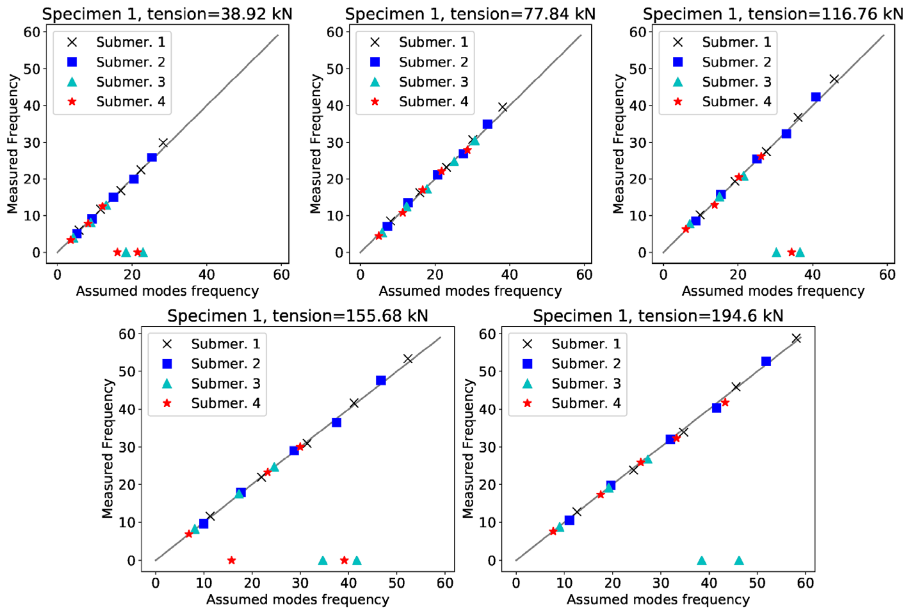

Fig. 9 Comparison of frequencies for specimen 1

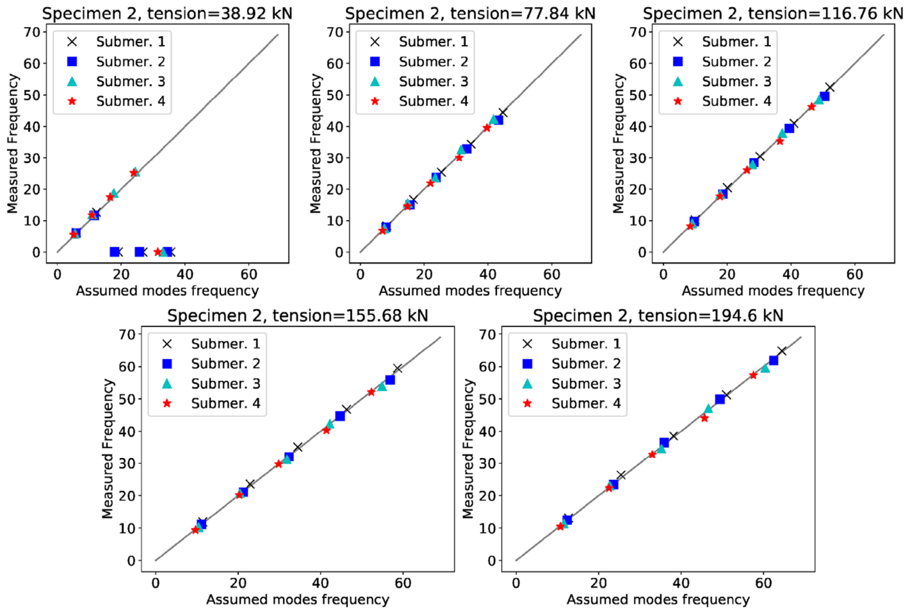

Fig. 10 Comparison of frequencies for specimen 2

provided on each plot for ready comparison; if the proposed method considering added mass does a good job of explaining the effects of submersion on the frequencies, then all points on the plots should lie near the y = x line. In each of the figures, the individual plots show the comparison for all levels of submersion for one level of pretension, with the levels of submersion represented by different point markers. The first five modes for each level of submersion are plotted simultaneously. Markers on the plot lying along a $y = 0$ line are those locations where a particular frequency could not be determined from the measured data, such as for the previously described scenario for the test of specimen 1 at 155.69 kN (35.0 kips) and 335 cm (132 in) of water.

As seen in the figures, considering only the added mass due to the presence of water adequately describes the effects of submersion on the fundamental frequency. That is, the estimated frequency using the assumed modes shape matches very closely to the measured frequency. A quantitative assessment of the error between the modeled frequencies and measured frequencies is shown in Fig. 12. The colors in the figure represent the different levels of tension, while the different markers represent the different submersion levels. As seen, with a few outliers, the estimated frequencies are generally within 5% error of the measured frequency, and often less than 5%. For specimen 1, the error is evenly spread between overestimating and underestimating the measured frequency. For specimen 2,

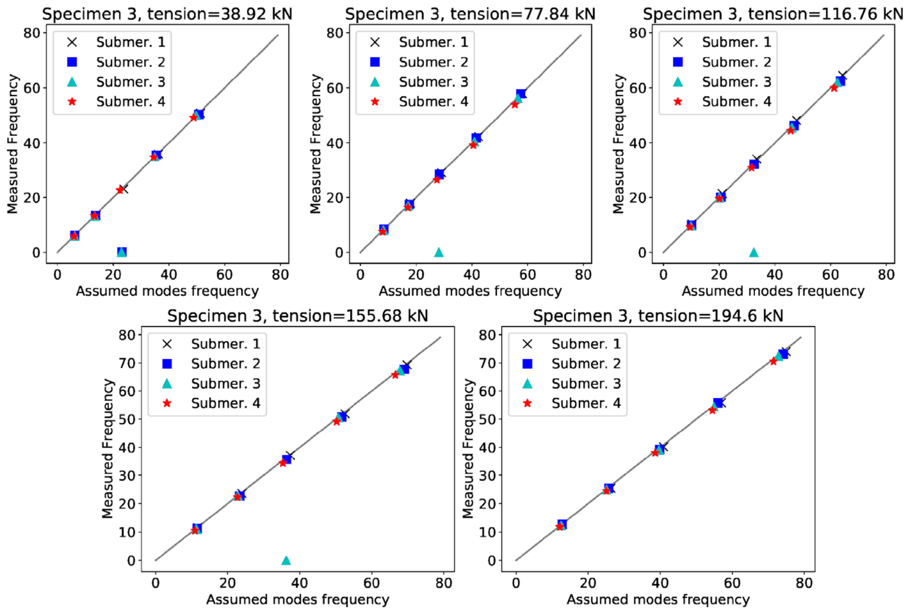

Fig 11 Comparison of frequencies for specimen 3

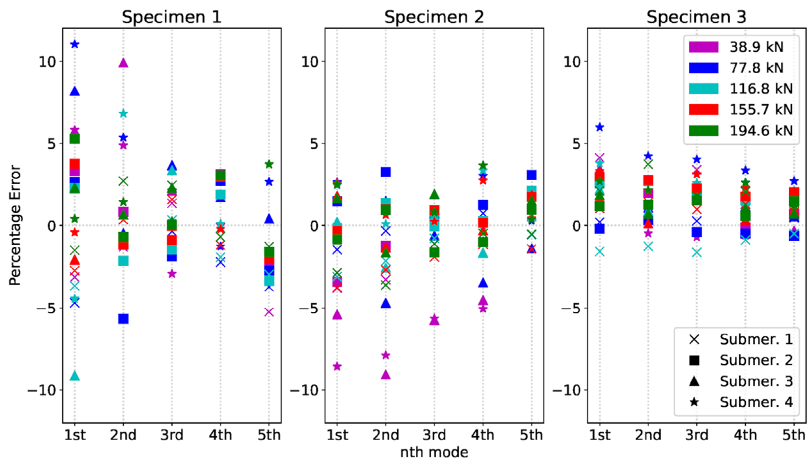

Fig 12 Percentage error between measured frequency and calculated frequency

the error tends to skew more towards an underestimation of the frequency. For specimen 3, the error tends to skew more towards an overestimation. The percentage error doesn't provide adequate information for the purposes of this study. The measured frequencies are to be used to calculate tension in the beams, where tension is related to the square of the frequency. Accordingly, it is important to investigate the magnitude of difference between the calculated and measured frequencies, as small differences in frequency can manifest as large errors in calculated tension. The difference in frequencies for the specimens are shown in Fig. 13. As seen, while the percentage error is generally high for the proposed approach when estimating the fundamental frequency, the magnitude of the difference in frequencies is the smallest for the fundamental frequency in all cases, and typically within 0.5 Hz. Accordingly, for this initial study, the tension is calculated by only considering the fundamental frequency. Future work will investigate the incorporation of higher modes to potentially increase accuracy.

As seen in the figures, considering only the added mass due to the presence of water adequately describes the effects of submersion on the fundamental frequency. That is, the estimated frequency using the assumed modes shape matches very closely to the measured frequency. A quantitative assessment of the error between the modeled frequencies and measured frequencies is shown in Fig. 12. The colors in the figure represent the different levels of tension, while the different markers represent the different submersion levels. As seen, with a few outliers, the estimated frequencies are generally within 5% error of the measured frequency, and often less than 5%. For specimen 1, the error is evenly spread between overestimating and underestimating the measured frequency. For specimen 2, the error tends to skew more towards an underestimation of the frequency. For specimen 3, the error tends to skew more towards an overestimation. The percentage error doesn't provide adequate information for the purposes of this study. The measured frequencies are to be used to calculate tension in the beams, where tension is related to the square

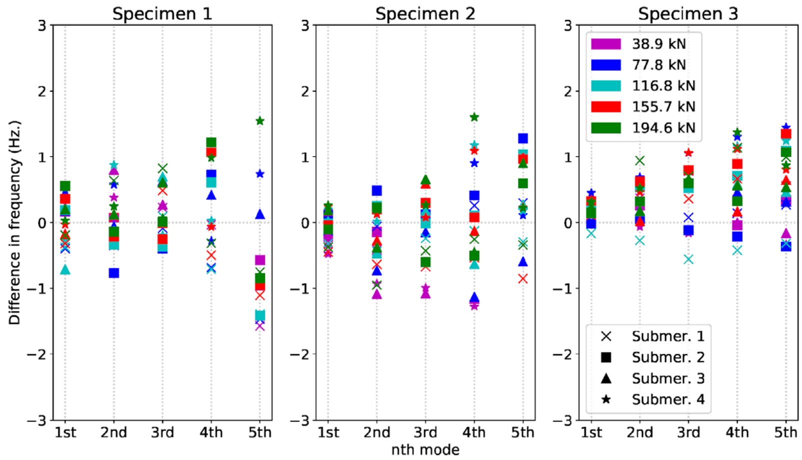

Fig 13 Difference of calculated frequency from measured frequency

of the frequency. Accordingly, it is important to investigate the magnitude of difference between the calculated and measured frequencies, as small differences in frequency can manifest as large errors in calculated tension. The difference in frequencies for the specimens are shown in Fig. 13. As seen, while the percentage error is generally high for the proposed approach when estimating the fundamental frequency, the magnitude of the difference in frequencies is the smallest for the fundamental frequency in all cases, and typically within 0.5 Hz. Accordingly, for this initial study, the tension is calculated by only considering the fundamental frequency. Future work will investigate the incorporation of higher modes to potentially increase accuracy.

While the results for the frequency comparison is promising, the primary interest of this study is to be able to measure the tension in a partially submerged miter gate diagonal by measuring only the diagonal dimensions, submerged length, and fundamental frequency of vibration. To find the tension given the measured parameters, an iterative inverse approach is used where the frequencies of vibration for a range of tension values given the submerged length are calculated. Then, the tension that corresponds to the calculated frequency that is nearest to the measured frequency for a given submersion length is used as the tension in the diagonal. This is performed for all test specimens and the tension value calculated using the proposed method is plotted versus the reference tension values in Fig. 14. The percentage error between the calculated tension and the measured tension is shown in Fig. 15. With a few exceptions (particularly for Specimen 1 at lower tension levels), the calculated tension is generally within 10% of the measured tension. The increased error seen in specimen 1 may be because the cross-section of the specimen is such that, without the geometric stiffness afforded by axial tension, the bending stiffness of the specimen is negligible. When the tension is low, Specimen 1 will have very little stiffness, and so the amplitude of vibration due to a hammer impact may violate the low-amplitude assumptions. The additional effects due to submersion (such as added damping) may need to be considered for improved accuracy for specimens with low tension and low bending stiffness, which will be explored in future work. Nevertheless, the proposed approach greatly improves the accuracy of calculations compared to neglecting the effects of submersion in water. For comparison, the percentage error in calculated tension when the effects of submersion are neglected are shown in Fig. 16. As seen, when neglecting the effects of submersion, the calculated tension values can be as much as 70% off. By utilizing the proposed method, tension can generally be calculated within a range likely to be acceptable to a practicing engineer.

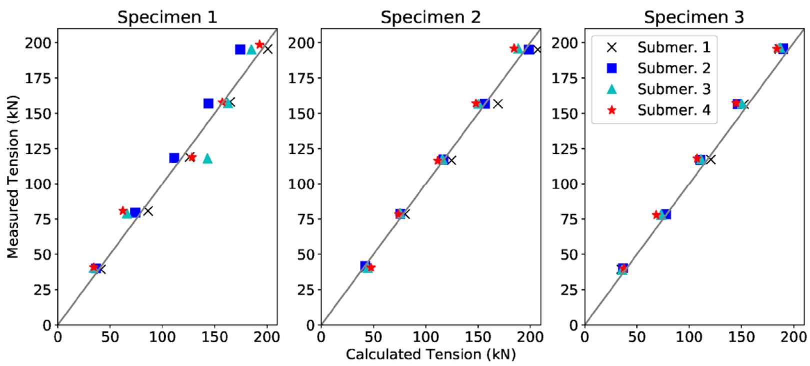

Fig. 14 Comparison of measured tension and calculated tension for test specimens

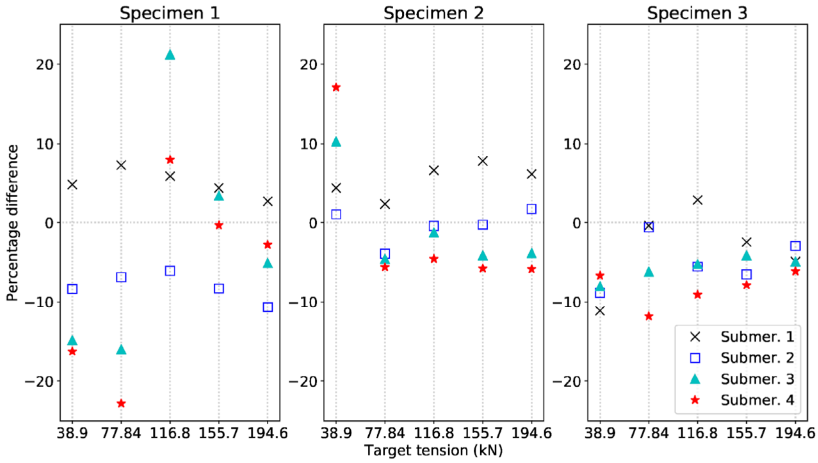

Fig. 15 Percentage error of calculated tension

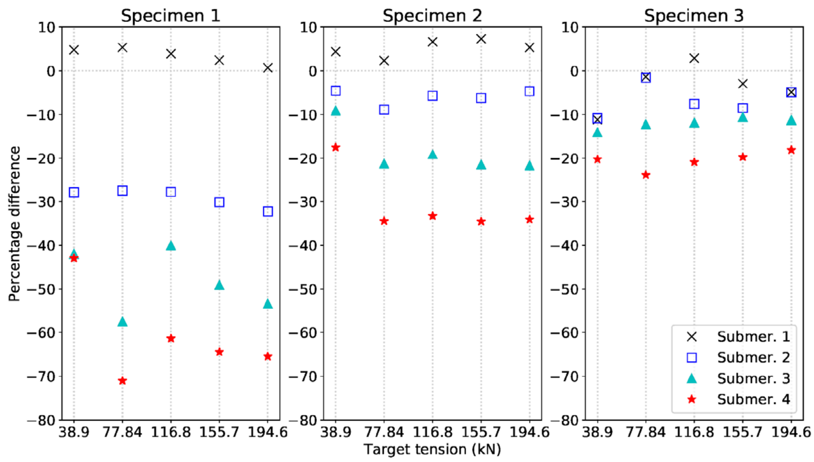

Fig. 16 Percentage error of calculated tension if effects of submersion not considered

5. Field validation

To test the efficacy of the proposed approach in the field, as well as validate the vision-based method proposed by Eick *et al*. (2020), video was taken of the diagonals of the Greenup Lock and Dam while it was in operation. The Greenup Lock and Dam site is on the Ohio River on the border of the U.S. state of Kentucky and Ohio, and is in the namesake county in the state of Kentucky. The miter gate at Greenup is the only known miter gate in the U.S. with instrumentation in place in the form of a load cell to monitor the tension in the diagonals, allowing the comparison of results found via the proposed approach with readings from the load cell. The same camera used in the lab was used in the field, and the camera was placed on a tripod on the lock chamber wall and pointed at the diagonals with a zoom lens. Fig. 17(b) shows the field-of-view of the camera in the field test, with the location of the field of view on the gate noted in Fig. 17(a).

Several videos were taken of the diagonals on the gate. The camera used on site was a Nikon DS3300 with a resolution of 1080p 60 fps and a focal length of 55 mm. Video results were improved with the use of a Nikon AF-S NIKKOR 70-200 mm f/2.8G ED VR II zoom lens. For the vision-based method to be effective, the best results were

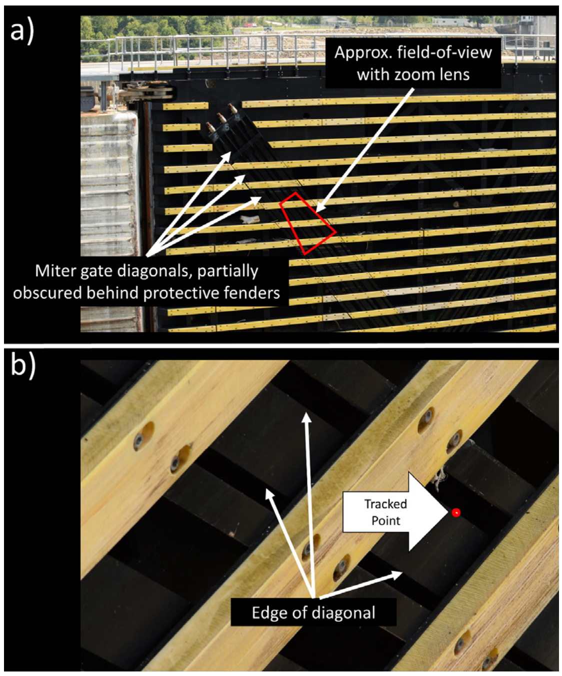

Fig. 17 (a) The Greenup miter gate on the day video was captured; (b) The field-of-view of the camera placed on the lock chamber wall

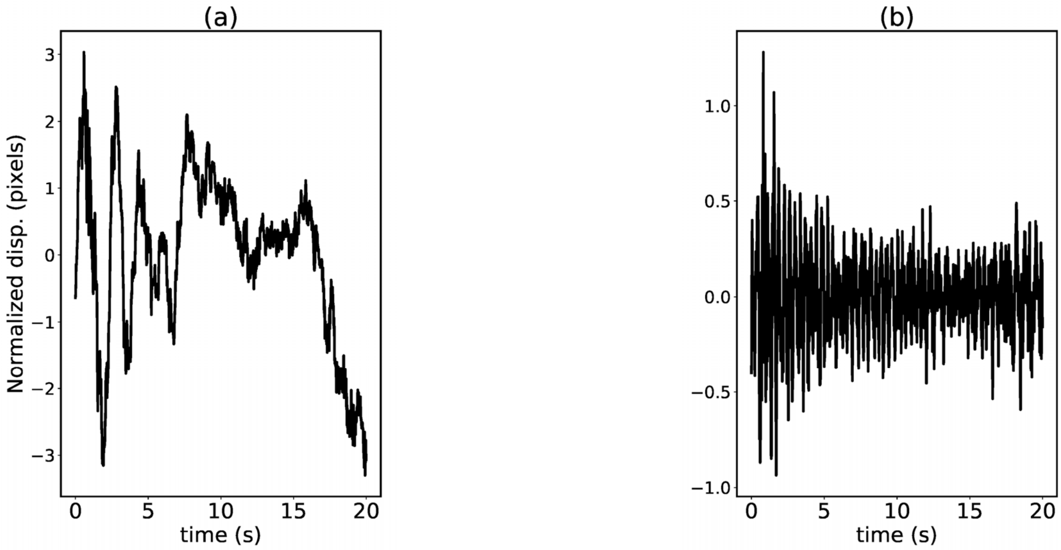

(a) Raw displacement of tracked point of Greenup diagonal (b) Filtered displacement of tracked point

Fig. 18 Displacement results from Greenup field testing

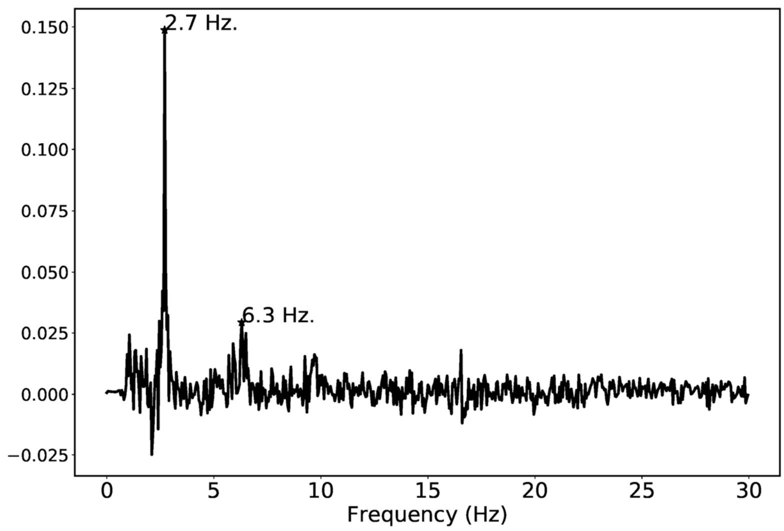

Fig. 19 FFT of displacement of Greenup diagonal

obtained as the gate swung closed and immediately after the two leaves of the gate came in contact with each other. This small impact provided adequate excitation to the diagonals for the optical flow method to track. The vision-based approach was applied to the captured video and the raw displacement record as tracked by optical flow is shown in Fig. 18(a). A high-pass Butterworth filter was applied to the displacement signal with a cutoff frequency of 1.0 Hz, and the filtered displacement record is shown in Fig. 18(b). An FFT was applied to the filtered displacement record to determine the frequencies of vibration. The resulting fundamental frequency is found to be 2.7 Hz, as shown in Fig. 19, while the second peak of 6.3 Hz is a reasonable value for the second harmonic of the beam.

The Greenup diagonals are 22.5 m (886.5 in.) in length, with a cross section of 17.8 cm × 3.18 cm (7.0 in. × 1.25 in). As one of the newer gates on the Ohio River, the diagonals utilize the same super-nut jackbolt connections as those tested in the lab, and so fixed-pinned boundary conditions are assumed. Using the proposed method, a vibration frequency of 2.7 Hz, and a length of submersion of 14.1 m (556 in), the tensile load is determined to be 895.2 kN (201.25 kips). The load cell on the diagonal read 862.9 kN (194 kips), resulting in an error of 3.7% for the proposed method. Note, using beam theory and ignoring the effects of submersion on the frequency of vibration, the tension in the diagonals is calculated to be 630.5 kN (141.75 kips), for an error of 26.9%

6. Conclusions

Miter gates are critical infrastructure to the U.S. economy that facilitate the transportation of billions of dollars in goods annually. Diagonals are long, slender, beam-like component of miter gates that are pre-tensioned to add torsional rigidity to the structure and counteract the tendency for the gate to twist under its own weight. Monitoring the tension in the miter gate diagonals is critically important for maximizing the useful life of the gate. Due to the expense and infeasibility of installing direct measurements of the tension of already in-service diagonals, vibration-based methods are attractive to infer the tension in the diagonal. Of particular challenge to calculating the tension from the frequency of vibration is the fact that miter gate diagonals will be partially submerged for most of their life.

The study conducted herein was performed to determine a simple method for calculating the tension in partially submerged miter gate diagonals given a measurement of the frequency of vibration and submerged length of the member. To this end, the effects of partial submersion on the frequency of vibration of the diagonal were investigated. The primary effect of submersion on the miter gate diagonal is found to be a reduction in the frequency of vibration due to added mass caused by the displacement of the water surrounding the diagonal. Closed-form solutions accounting for the added mass of a partially submerged diagonal are particularly challenging given that the submerged length of the diagonal is not constant. While a characteristic equation of the partially submerged diagonal can be found, numerically solving the characteristic equation for tension in the diagonal given the frequency of vibration and submerged length is intractable. Accordingly, the assumed modes method was used to calculate the frequency of vibration of a diagonal given a pretension and level of submersion.

Experimental data was then used to validate the notion that the effects of submersion on the frequency of vibration of the diagonal can be largely accounted for by added mass due to water. The experiment consisted of three scale-model diagonal specimens subjected to various levels of pretension and submersion. The scale model specimens were excited and the first five frequencies of vibration were calculated from the displacement record. In all cases, the experimentally obtained frequencies of vibration matched the calculated frequencies obtained using the assumed modes. The exceptional agreement in the data corroborates the notion that the primary effect of submersion of the frequency can be modeled as added mass. To calculate the tension in the specimens using the measured frequency and submerged length of the beam, an iterative inverse approach is utilized where frequencies of vibration are generated for several tension values given a length of submersion. Then, the tension that matches the combination of submerged length and nearest value of frequency of vibration is taken as the tension in the beam

Field validation was performed by utilizing vision-based vibration measurement of an in-service miter gate diagonal at the Greenup Lock and Dam. The diagonals at the Greenup Lock and Dam are instrumented with load cells to monitor the tension in the diagonals, allowing for comparison of the tension found via the proposed method with that recorded by the load cell. The tension calculated using the proposed method showed excelled agreement, differing from the load cell by only 3.7%. This field validation showed that the proposed method discussed herein is viable for monitoring tension in miter gate diagonals. While the results of this study focus on miter gate diagonals, the results can easily be utilized on any other long, slender, pre-tensioned, partially submerged beams.

Acknowledgments

The authors would like to thank: Yasutaka Narazaki for providing the video used for the field validation portion of this study; USACE Huntington District, in particular the personnel on site at the Greenup Lock and Dam for their assistance in the acquisition of the video used in this study; Fernando Gomez for his suggestion to try Chebyshev polynomials for the assumed modes method.

References

Chen, S.S. (1985), *Flow-induced vibration of circular cylindrical structures*, Argonne National Laboratory, Report No. ANL-85-51, Argonne, IL, USA.

Craig Jr, R.R. and Kurdila, A.J. (2006), *Fundamentals of Structural Dynamics*, John Wiley and Sons, Hoboken, NJ, USA.

Eick, B.A., Narazaki, Y., Smith, M.D. and Spencer Jr, B.F. (2020), “Vision-based monitoring of post-tensioned diagonals on miter lock gates”, *J. Struct. Eng.*, **146**(10), 04020209. 10.1061/(ASCE)ST.1943-541X.0002777

Feng, D., Scarangello, T., Feng, M.Q. and Ye, Q. (2017), “Cable tension force estimate using novel noncontact vision-based sensor”, *Measurement*, **99**, 44-52. 10.1016/j.measurement.2016.12.020

Hoffmann, E.G. (1944), “Torsional Deflection of Miter-Type Lock Gates and Design of the Diagonals”, Master’s Thesis, Washington University in St. Louis, MO, USA.

Jang, S., Jo, H., Cho, S., Mechitov, K., Rice, J.A., Sim, S.H., Jung, H.J., Yun, C.B., Spencer Jr, B.F. and Agha, G. (2010), “Structural health monitoring of a cable stayed bridge using wireless smart sensor technology: data analysis”, *Smart Struct. Syst., Int. J.*, **6**(5-6), 461-480. 10.12989/sss.2010.6.5_6.461

Kaneko, S., Nakamura, T., Inada, F., Kato, M., Ishihara, K., Nishihara, T., Mureithi, N.W. and Langthjem, M.A. eds. (2014), *Flow-Induced Vibrations: Classifications and Lessons From Practical Experiences*, Elsevier, New York, NY, USA.

Kim, S.W. and Kim, N.S. (2013), “Dynamic characteristics of suspension bridge hanger cables using digital image processing”, *NDT&E* **59**, 25-33. 10.1016/j.ndteint.2013.05.002

Lepidi, M., Gattulli, V. and Vestroni, F. (2007), “Static and dynamic response of elastic suspended cables with damage”, *Int. J. Solids Struct.*, **44**(25-26), 8194-8212. 10.1016/j.ijsolstr.2007.06.009

Lepidi, M., Gattulli, V. and Vestroni, F. (2009), “Damage identification in elastic suspended cables through frequency measurement”, *J. Vib. Control*, **15**(6), 867-896. 10.1177/1077546308096107

Mason, J.C. and Handscomb, D.C. (2003), *Chebyshev Polynomials*, Chapman & Hall/CRC, Boca Raton, FL, USA.

Rao, S.S. (2007), *Vibrations of Continuous Systems*, John Wiley and Sons, Hoboken, NJ, USA.

Riveros, G.A., Ayala-Burgos, J.L. and Dixon, D. (2017), “Numerical investigation of diagonals in miter gates: looking for the optimum prestressing”, *J. Perform. Constr. Facil.*, **31**(1),

0401607.
10.1061/(ASCE)CF.1943-5509.0000896
Rytter, A. (1993), "Vibration Based Inspection of Civil Engineering Structures", Thesis; Aalborg University, Denmark.
Shaker, F.J. (1975), *Effect of Axial Load on Mode Shapes and Frequencies of Beams* (*NASA TN D-8109*), NASA, Washington D.C., USA.
Shermer, C.L. (1957), "Stiffening lock gates by prestressing diagonals", *Proceedings of the American Society of Civil Engineers*, **81**(9), 1-10.
U.S. Army Corps of Engineers (1994), Engineering and Design: Lock Gates and Operating Equipment; EM 1110-2-2703, Washington D.C., USA.